

Interlayer structures of the chiral smectic liquid crystal phases revealed by resonant x-ray scattering

L. S. Hirst, S. J. Watson, and H. F. Gleeson*

Department of Physics and Astronomy, University of Manchester, Manchester M13 9PL, United Kingdom

P. Cluzeau

Bâtiment P5, University Lille 1, F-59655 Villeneuve d'Ascq Cedex, France

P. Barois

Centre de Recherche Paul Pascal, CNRS, Université de Bordeaux I, Avenue A. Schweitzer, F-33600 Pessac, France

R. Pindak and J. Pitney

Lucent Technologies, Bell Laboratories, Murray Hill, New Jersey 07914

A. Cady, P. M. Johnson, and C. C. Huang

School of Physics and Astronomy, University of Minnesota, Minneapolis, Minnesota 55455

A-M. Levelut

Laboratoire de Physique des Solides, Université Paris-Sud, F-91405 Orsay, France

G. Srajer and J. Pollmann

APS, Argonne National Laboratory, Argonne, Illinois 60439

W. Caliebe

NSLS, Brookhaven National Laboratory, Upton, New York 11973

A. Seed and M. R. Herbert

Liquid Crystal Institute, Kent State University, Kent, Ohio 44240

J. W. Goodby and M. Hird

Department of Chemistry, Hull University, Hull HU6 7RJ, United Kingdom

(Received 5 November 2001; published 2 April 2002)

The structures of the liquid crystalline chiral subphases exhibited by several materials containing either a selenium or sulphur atom have been investigated using a resonant x-ray scattering technique. This technique provides a unique structural probe for the ferroelectric, ferrielectric, antiferroelectric, and SmC_α^* phases. An analysis of the scattering features allows the structural models of the different subphases to be distinguished, in addition to providing a measurement of the helical pitch. This paper reports resonant scattering features in the antiferroelectric hexatic phase, the three- and four-layer intermediate phases, the antiferroelectric and ferroelectric phases and the SmC_α^* phase. The helicoidal pitch has been measured from the scattering peaks in the four-layer intermediate phase as well as in the antiferroelectric and ferroelectric phases. In the SmC_α^* phase, an investigation into the helical structure has revealed a pitch ranging from 5 to 54 layers in different materials. Further, a strong resonant scattering signal has been observed in mixtures of a selenium containing material with as much as 90% nonresonant material.

DOI: 10.1103/PhysRevE.65.041705

PACS number(s): 61.30.Eb

I. INTRODUCTION

Smectic liquid crystals consist of a layered molecular arrangement and exist in several variant phases. The best known of these phases is the ferroelectric (SmC^*) phase [1], in which the tilted chiral molecules in the smectic layers will respond to the application of an electric field by reversing their molecular electric polarization direction. The other Sm

C^* variant phases are also tilted and differ from each other in the precession of molecular orientation from layer to layer. The SmC^* subphases all exhibit a macroscopic helix, as a result of the molecular chirality. The pitch of this helix varies from phase to phase and is typically several hundred layers in size.

The antiferroelectric phase (SmC_A^*) was first observed in liquid crystals in 1989 [2] and this phase also demonstrates significant potential for device applications. The antiferroelectric (SmC_A^*) liquid crystal phase is formed when the molecules in alternate layers tilt in opposite directions, the

*Author to whom correspondence should be addressed.

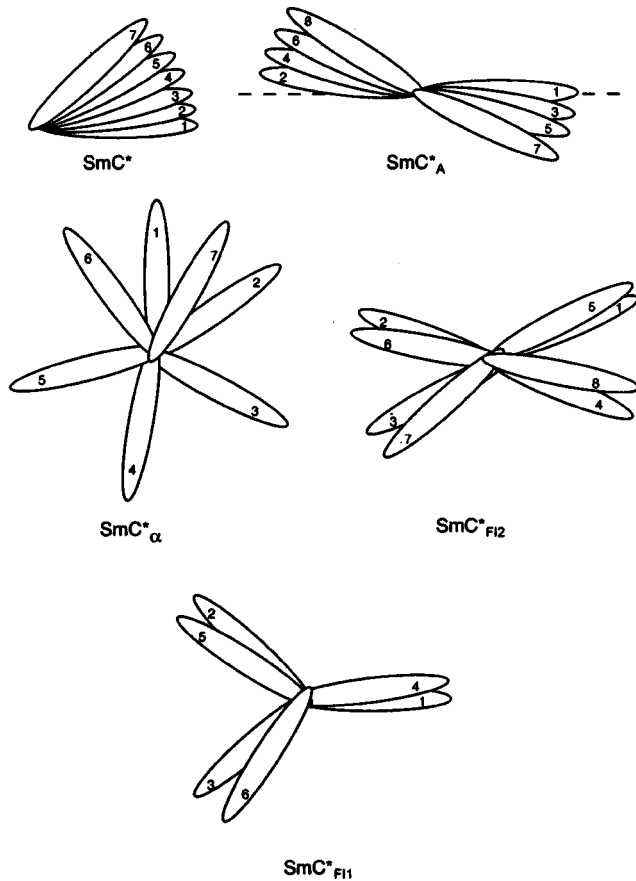


FIG. 1. The SmC^* subphase structures. The diagram shows how the azimuthal angle varies in each phase, the numbered molecules demonstrating the progression in molecular orientation through a sequence of consecutive layers as viewed from above.

dipole contribution also reversing in direction from one layer to the next. In addition to the SmC_A^* phase, several different SmC^* subphases have been identified and studied [3]. The ferroelectric $\text{SmC}_{\text{F11}}^*$ phase, intermediate four-layer $\text{SmC}_{\text{F12}}^*$ phase, ferroelectric SmC^* phase, and the complex SmC_α^* phase can all exist between the SmC_A^* phase and the untitled Sm A phase. These phases exhibit different interlayer molecular arrangements and display a variety of interesting electrical and optical properties (Fig. 1).

Although the different chiral subphases have been studied since the early 1990s, the molecular ordering in these phases is still an area ripe for research. The structure of the intermediate (ferroelectric) phases has, for several years, been a controversial subject. Conventional x-ray scattering can provide no information on repetitions in molecular orientation, the feature that distinguishes the SmC^* subphases. As a result, several different models have been proposed [2,4,5] to explain the properties of these phases. The technique of resonant scattering has been used in the field of crystallography [6] and now has proven to be a valuable tool in liquid crystal science.

Resonant scattering is an x-ray technique that involves tuning the x-ray energy near the absorption edge of an atom contained within the core of the liquid crystal molecule. Conventional x-ray scattering probes variations in electron

density in the sample, whereby peaks are observed at $Q_z = 2\pi l/d = lQ_o$, where l is an integer and d is the smectic layer spacing. Near the absorption edge energy, the structure factor of the material becomes a tensor [7] and the scattering becomes sensitive to molecular orientation. The value of this tensor is dependent on the orientation of the molecule with respect to the polarization direction of the x-ray beam, so extra resonant peaks are observed where there is a superlattice structure of molecular orientations and the different phases can be distinguished [8].

The positions of the resonant peaks in each phase can be calculated using the equation,

$$Q_z/Q_o = l + m \left[\left(\frac{1}{\nu} \right) + \varepsilon \right], \quad (1)$$

where l is an integer, m can take integer values between ± 2 , ν is the superlattice periodicity (in layers), and ε is given by the ratio of the smectic layer spacing d and the optical pitch P_0 .

The SmC^* subphases were first investigated in this way by Mach *et al.* [9,10] demonstrating the clock model [11] of the three- and four-layer intermediate phases to be their most likely structure. Ellipsometry work by Johnson *et al.* [12] demonstrated that the correct molecular arrangements should be a biaxial distorted clock structure. Subsequently, this model was confirmed by an in-depth study of the four-layer $\text{SmC}_{\text{F12}}^*$ phase using high resolution resonant scattering [13], providing evidence for the asymmetric clock structure proposed by Lorman [14], thus revealing the true structure of the phase (which is not ferroelectric, despite commonly being labeled as such). Resonant scattering studies have also been carried out in liquid crystal devices [15] allowing the study of interlayer structures under the influence of electric fields.

The structure of the SmC_α^* subphase has, for a long time, remained a controversial subject. Before the first successful resonant scattering experiment [10] this phase was known to be a small tilt smectic phase [16], exhibiting either ferroelectric or antiferroelectric electro-optic behaviors [3,17]. The existence of a small optical periodicity in the SmC_α^* phase was first reported in 1996. The authors attributed this periodicity to a helical structure similar to the SmC^* phase, but with a shorter pitch [18,19]. Optical reflectivity [20] and ellipsometry [12] measurements on free-standing films have also provided interesting information on the SmC_α^* phase revealing a film consisting of a tight pitch helix with antiferroelectric surface regions. Resonant scattering has been particularly useful in precisely deducing the structure of the SmC_α^* phase. Indeed, the analysis of satellites to the Bragg peak in the first experiment on compound VI [9] (Fig. 2) has shown a superlattice periodicity incommensurate with the layer spacing. In this material the periodicity has been shown to evolve from roughly eight to five layers upon decreasing the temperature. The incommensurate periodicity of about five layers just above the $\text{SmC}_{\text{F12}}^*$ phase would suggest that the SmC_α^* phase is a natural extension of the $\text{SmC}_{\text{F12}}^*$ phase, although it is true that if a material exhibits the SmC^* phase

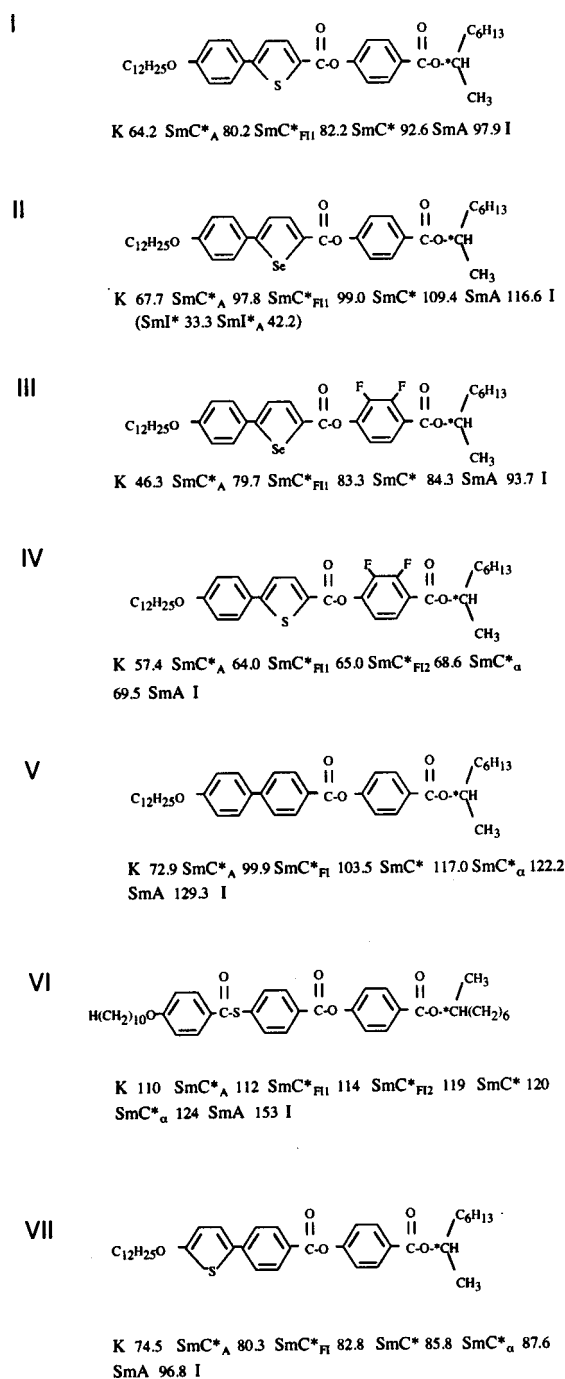


FIG. 2. The molecular structures and phase sequences of the materials studied. All transition temperatures are in degrees centigrade and were determined by microscopy and electro-optic measurements.

in addition to the SmC*_{F12} and SmC*_α phases, then the SmC* phase will always occur beneath the SmC*_α phase.

This paper presents a comprehensive investigation of the SmC* subphases in several materials using the resonant x-ray scattering technique. A total of six different chiral smectic phases have been studied and resonant scattering features characteristic of each phase are presented. Where possible, measurements of the helicoidal pitch of the phase

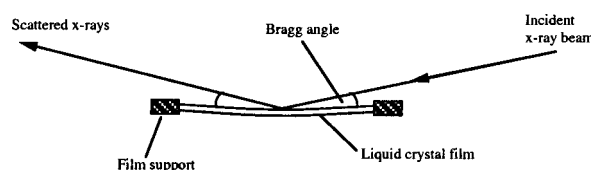


FIG. 3. The scattering geometry for liquid crystal free-standing films. The Bragg angle is typically 0.8° for Se and 4.1° for S. The free-standing films contain approximately 500 layers, so have a thickness of around $1.7 \mu\text{m}$.

have been made from the resonant scattering data and these are also presented.

One potential restriction of the resonant scattering technique is that in order for it to be useful, the material under investigation must contain a suitable atom (e.g., sulfur, selenium, silicon, bromine, etc.). In this paper, resonant x-ray scattering data are also presented for mixtures of two materials, one of which does not contain a resonant atom. These data demonstrate how resonant signals can be observed in mixtures containing low concentrations of resonant material. This additional application demonstrates the broad potential of resonant x-ray scattering for use in the study of a wide variety of liquid crystalline systems.

II. EXPERIMENT

Resonant x-ray scattering studies have been performed on several antiferroelectric liquid crystal materials, which have also been described elsewhere [9,10,13]. The molecular structures of the compounds examined in this work are shown in Fig. 2 together with their phase sequences determined by optical microscopy and electro-optic techniques. It should be noted that the chiral smectic subphases always exist in the same order on increasing or decreasing the temperature, but that not all phases are present in all materials.

The x-ray studies of selenium containing materials were carried out at the Advanced Photon Source (APS) at Argonne National Laboratories, II, and the sulfur containing materials were studied at the National Synchrotron Light Source (NSLS) at Brookhaven National Laboratories, NY. These facilities provided the high flux, tunable sources necessary for this work.

Thick film samples were prepared by spreading liquid crystal material, heated to the SmA phase, across a circular hole, 1 cm diameter in a stainless steel film plate. When a smectic liquid crystal forms a free-standing film, the molecules arrange themselves so that the layers lie parallel to the film plate. This homeotropic arrangement provides an excellent alignment for x-ray scattering studies (Fig. 3) and no substrate is required to contain the material. The film plate was situated within a double stage oven system, which could be flushed with inert gas. This oven provided a controlled environment with a relative temperature accuracy of 0.01 K. The oven and flight path were flushed with helium to reduce air scatter. A schematic of the flight path is shown in Fig. 4.

It was possible to create thick films across the hole by spreading the liquid crystal material very slowly across the film plate in the oven. Typically, films were formed with a

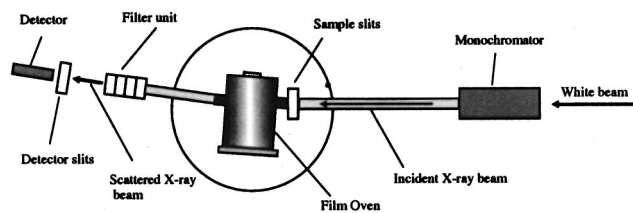


FIG. 4. A schematic representation of the flight path in the x-ray apparatus.

thickness of about 500 smectic layers. A thick film was required to produce a large enough scattering intensity to resolve the weak resonant features. The thickness of the film was verified by observing the film color when illuminated by white light. The sample could be viewed using a telescope, angled through a glass window in the top of the oven. This experimental arrangement allowed the liquid crystal film textures to be monitored remotely during experiments. Such a viewing system was vital as it allowed the verification of a uniform film texture; the footprint of the x-ray beam on the film is large at grazing incidence and the simultaneous existence of more than one phase would produce unreliable results. The telescope also allowed the observation of phase transitions in the film as the oven temperature was changed.

In order to detect a resonant scattering signal, the x-ray beam was tuned to the energy yielding the maximum intensity of the fluorescence spectrum, which is near the K -absorption edge of the suitable atom in the molecular core. Measured fluorescence spectra emissions are shown in Fig. 5 for compounds I and II that contain sulfur and selenium, respectively.

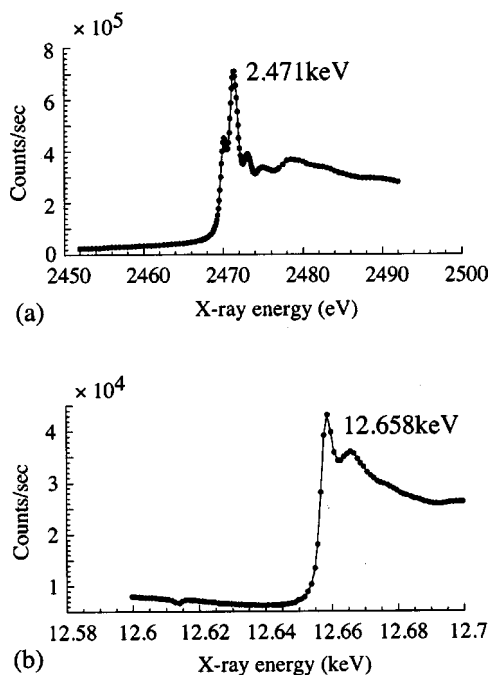


FIG. 5. Fluorescence spectra of the K -absorption edge for (a) compound I (sulfur) and (b) compound II (selenium).

III. RESULTS AND DISCUSSION

The clock model [5] can be distinguished from the Ising model [3] in the SmC^* subphases by a study of the polarization of first and second order resonant peaks. For a clock model, the first order resonant peaks should be π polarized and the second order peaks σ polarized for a σ polarized incident x-ray beam in the $\text{SmC}_{\text{FI1}}^*$ and $\text{SmC}_{\text{FI2}}^*$ phases, whereas the Ising model predicts σ -polarized first order peaks in these phases. As well as providing information regarding the structural details of the phases, the separation of the resonant peaks can be used to give a measurement of the pitch of the macroscopic helix. Peak positions can be predicted using Eq. (1). Peak intensities cannot be compared between separate scans for these measurements, as the data have not been normalized against beam intensity.

A. The antiferroelectric phase

All of the materials examined exhibited an enantiotropic antiferroelectric phase above the crystalline state. A monotropic, hexatic antiferroelectric phase also exists in compound II beneath the SmC_A^* phase [21,22]. The positions and fine structure of the peaks observed can be related to the theory of resonant scattering for an antiferroelectric phase as follows. Theory predicts [8] that in the antiferroelectric phase, split resonant peaks will occur at $Q_z/Q_0 = l + \frac{1}{2} \pm \epsilon$ (where l is an integer) and second order satellite peaks at $Q_z/Q_0 = 1 \pm 2\epsilon$. Figure 6 shows details of resonant scattering results obtained in two different antiferroelectric liquid crystal phases. The $Q_z/Q_0 = 1.5 \pm \epsilon$ peaks are shown in the conventional antiferroelectric phase for compounds I, II, and III, and they were also observed in compound VI. In addition, satellite peaks at $Q_z/Q_0 = 2 \pm 2\epsilon$ were seen in compound I [Fig. 6(b)] and measured to have σ polarization, in contrast to the π polarization of the first order peaks. By cooling the film rapidly into the monotropic, hexatic antiferroelectric phase in compound II it was also possible to observe antiferroelectric ordering in this phase from peaks at $Q_z/Q_0 = l + \frac{1}{2}$, as can be seen from Fig. 6(e).

Using Eq. (1) the pitch in the film can be easily calculated at any particular temperature as the diffraction peak splitting is clearly defined in the SmC_A^* phase. The helicoidal pitch in the antiferroelectric liquid crystalline phases calculated from the data in Fig. 6 are (a) and (b) $0.432 \mu\text{m}$, (c) $0.186 \mu\text{m}$, and (d) $0.534 \mu\text{m}$. On cooling compound II to observe the hexatic phase, the split peaks at $Q_z/Q_0 = 1.5 \pm \epsilon$ were observed to move closer together, indicating an increase in pitch in the system. The peaks appeared to converge at the transition into the hexatic phase, though a single resonant peak was still observable at $Q_z/Q_0 = 1.5$, confirming the antiferroelectric structure of this hexatic phase [Fig. 6(e)].

One drawback of the resonant scattering technique is the fact that most liquid crystalline materials do not contain a suitable resonant atom in the molecular core. The possibility of overcoming this problem has been investigated by doping nonresonant materials with a small amount of resonant material. Compound V was mixed with compound II in the proportions 50:50, 75:25, and 90:10, then films were drawn using these mixtures and scattering performed in the same

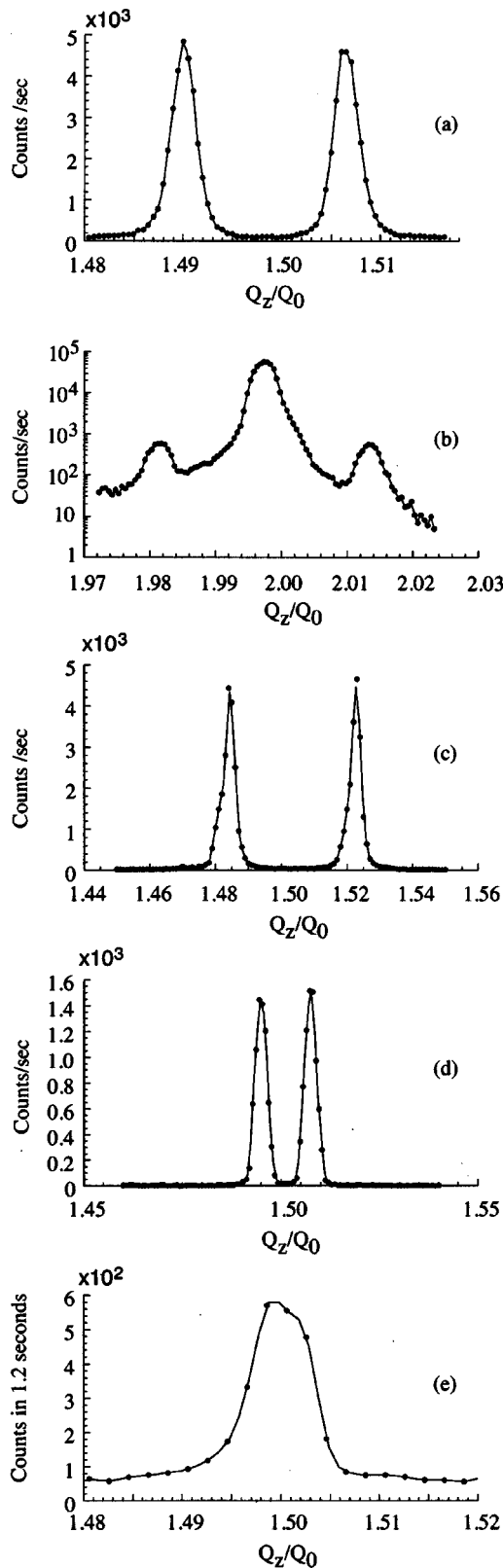


FIG. 6. Antiferroelectric resonant peaks for (a) compound I, first order peaks at $Q_z/Q_0=1.5$, (b) compound I, second order peaks at $Q_z/Q_0=2.0$, (c) compound III, first order peaks at $Q_z/Q_0=1.5$, (d) compound II, first order peaks about $Q_z/Q_0=1.5$, (e) compound II, first order peaks in the hexatic phase at $Q_z/Q_0=1.5$.

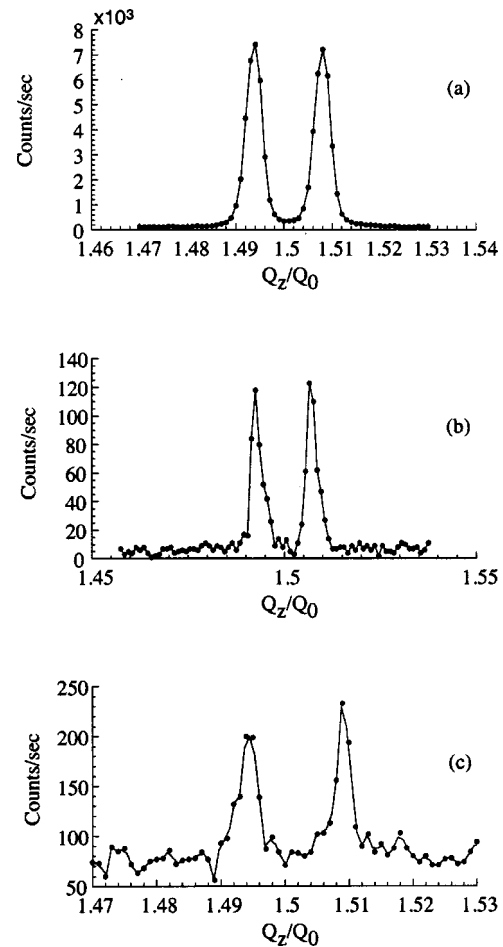


FIG. 7. Antiferroelectric resonant peaks observed around $Q_z/Q_0=1.5$ in mixtures of compound V with compound II. The ratios are (a) 50:50, (b) 75:25, and (c) 90:10.

way as described above. A clear resonant signal was obtained in the antiferroelectric phase in all of the mixtures, as shown in Fig. 7. The resonant features are still clear in the mixture containing the smallest proportion of the resonant material [Fig. 7(c)] and it seems reasonable to assume that even smaller amounts of dopant could be used for this technique. The smallest proportion of resonant material it is feasible to use is currently under investigation.

B. The intermediate phases

For all the materials studied here, the intermediate (FI) phase was present in at least one of its two known forms, denoted $\text{Sm } C_{\text{FI1}}^*$ (the ferrielectric three-layer structure) and $\text{Sm } C_{\text{FI2}}^*$ (the four-layer phase). In 1999 [9], it was demonstrated by a polarization analysis of resonant scattering data on compounds I and VI, that the most likely model for the structure of the FI phases was the clock model. In these compounds, this phase was shown to exist in two forms, a three-layer structure and a four-layer structure. The $\text{Sm } C_{\text{FI1}}^*$ phase, consisting of a three-layer superlattice, occurs at a lower temperature than the four layer, $\text{Sm } C_{\text{FI2}}^*$ phase but these phases both show a similar optical texture. Prior to the

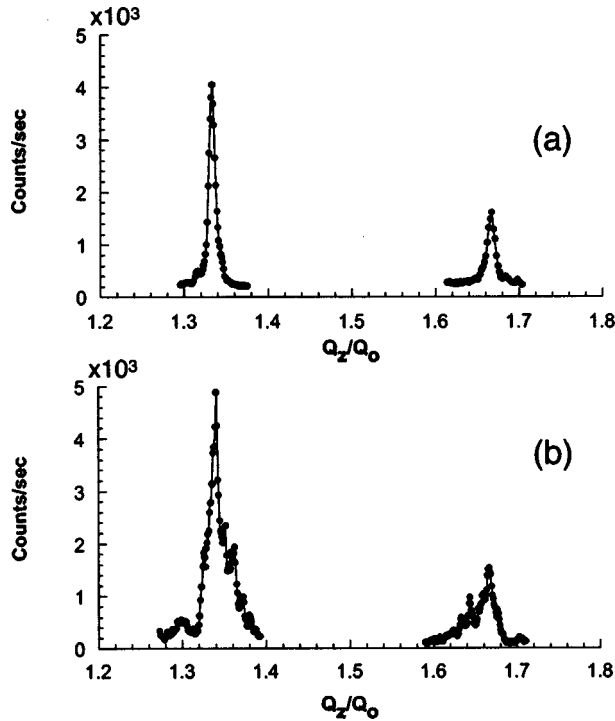


FIG. 8. Resonant peaks in the three-layer ferrielectric phase in (a) compound II and (b) compound III.

resonant scattering experiments, this similarity had made characterization and differentiation between the two phases difficult.

Theoretical predictions of resonant scattering features for the $\text{SmC}_{\text{FI1}}^*$ phase give peaks at $Q_z/Q_0 = l + \frac{1}{3} + \varepsilon$ and $Q_z/Q_0 = l + \frac{1}{3} - 2\varepsilon$ and also at $Q_z/Q_0 = l + \frac{2}{3} - \varepsilon$ and $Q_z/Q_0 = l + \frac{2}{3} + 2\varepsilon$. Such resonant peaks were observed in compounds II and III, as shown in Fig. 8, although it was not possible to observe any splitting due to the macroscopic helix at these positions. The absence of splitting may be due to the existence of a very long pitch in this phase, resulting in a peak separation less than the resolution of the scattering experiment (typically $\Delta Q_z = 1 \times 10^{-3} Q_z$). The second order peak in each pair will be much less intense than a first order one, thus contributing to the difficulty in observing this feature.

In the $\text{SmC}_{\text{FI2}}^*$ phase, resonant peaks are predicted at $Q_z/Q_0 = l + \frac{1}{4} + \varepsilon$, $l + \frac{1}{2} \pm 2\varepsilon$, and $l + \frac{3}{4} - \varepsilon$. Peaks corresponding to the $\text{SmC}_{\text{FI2}}^*$ phase have been observed in compounds III, IV, and VI, as shown in Fig. 9. It can be seen that the second order peak at $Q_z/Q_0 = 1.5$ is much less intense than its neighbors. In compound III [Fig. 9(a)] it was possible to resolve splitting in this weak peak at $Q_z/Q_0 = 1.5$ giving a measure for pitch in the four-layer phase of approximately $2.8 \mu\text{m}$. This value for the pitch is in good qualitative agreement with the values of $3\text{--}5 \mu\text{m}$ quoted by Akizuki *et al.* [23] for a different material in the high temperature intermediate phase.

Splitting of the first order resonant peaks has been resolved to reveal the asymmetric clock structure previously demonstrated by ellipsometric studies [12] and predicted by

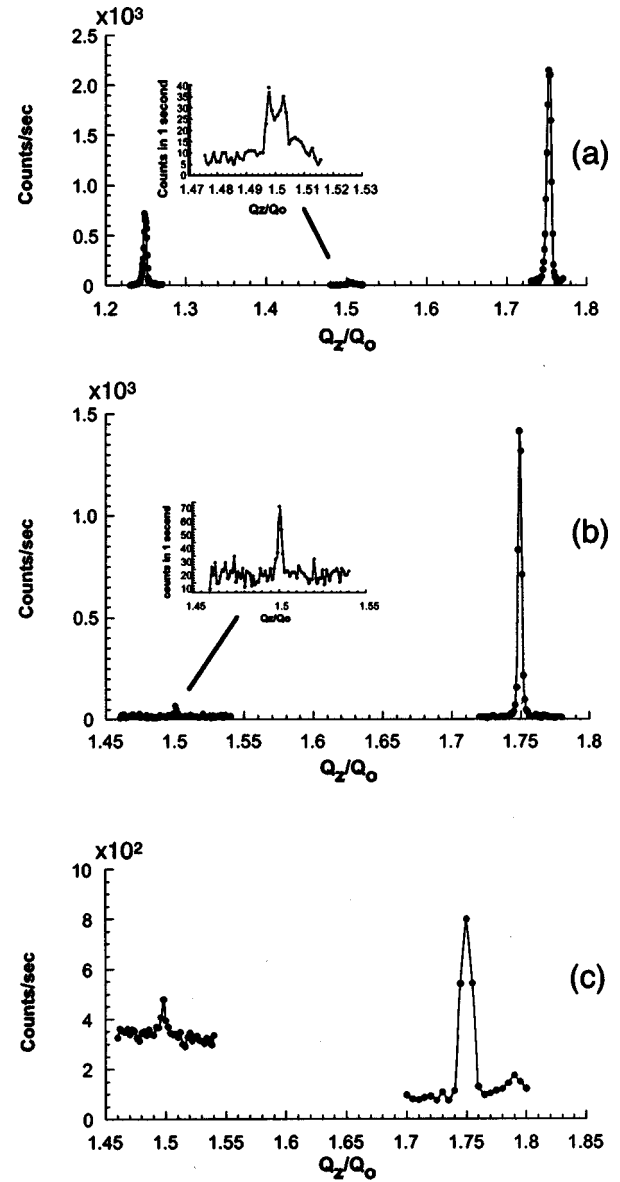


FIG. 9. Resonant peaks in the four-layer intermediate phase in (a) compound III, (b) compound IV, and (c) compound VI.

Lorman [14]. These findings have been reported in Ref. [13].

C. The ferroelectric phase

In the SmC^* phase, two sets of satellite peaks are predicted around the Bragg peaks and these have been observed around the $(0,0,2)$ peak in compounds I, II, and VI, as shown in Fig. 10. The spacing of these peaks again provides a measure of the pitch in each material. From the results presented, the pitch has been calculated as $0.320 \mu\text{m}$ at 87.5°C in compound I [Fig. 10(a)], $0.388 \mu\text{m}$ at 104.2°C in compound II [Fig. 10(b)], and $0.386 \mu\text{m}$ at 119.2°C in compound VI [Fig. 10(c)].

D. The SmC_α^* phase

Resonant scattering has proved to be particularly useful in deducing the structure of the rather complex SmC_α^* phase.

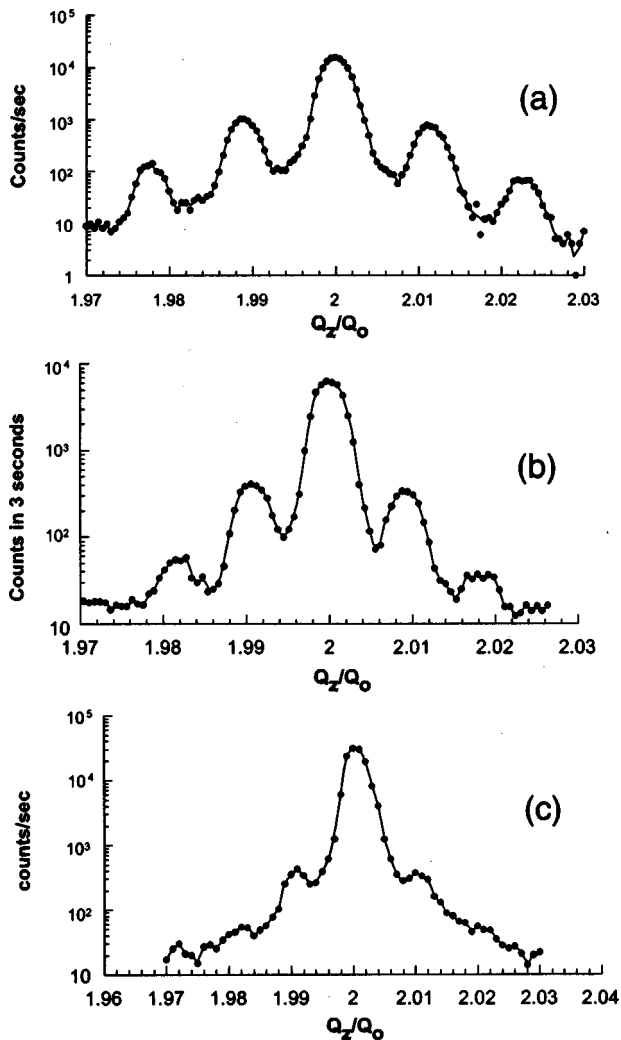


FIG. 10. Resonant satellites in the SmC^* phase about $Q_z/Q_0 = 2.0$ in (a) compound I, (b) compound II, and (c) compound VI.

Previous work [9] has shown that the phase has a superlattice periodicity incommensurate with pitch and that this periodicity varies with temperature across the phase. This result was deduced from observations of the first order resonant peaks in compound VI. Superlattice periodicity in the SmC^*_α phase can again be calculated by the use of Eq. (1). Resonant scattering from the SmC^*_α phase has now been observed in two new materials, compounds IV and VII, as shown in Figs. 11 and 13, respectively. A superlattice periodicity of $\nu = 5.1$ can be calculated from the data presented. In addition, more details have been observed in the resonant features of compound VI. Figure 11(c) shows second order satellites, which have been observed in the SmC^*_α phase. The position of these peaks is consistent with theoretical predictions.

In order to understand the thermal behavior of the superlattice periodicity through the SmC^* to SmC^*_α phase transition, a resonant scattering experiment was performed on a new thiophene material (compound VII), exhibiting a relatively large temperature range SmC^* phase below the SmC^*_α phase. The phase sequence and transition temperatures can be seen in Fig. 2.

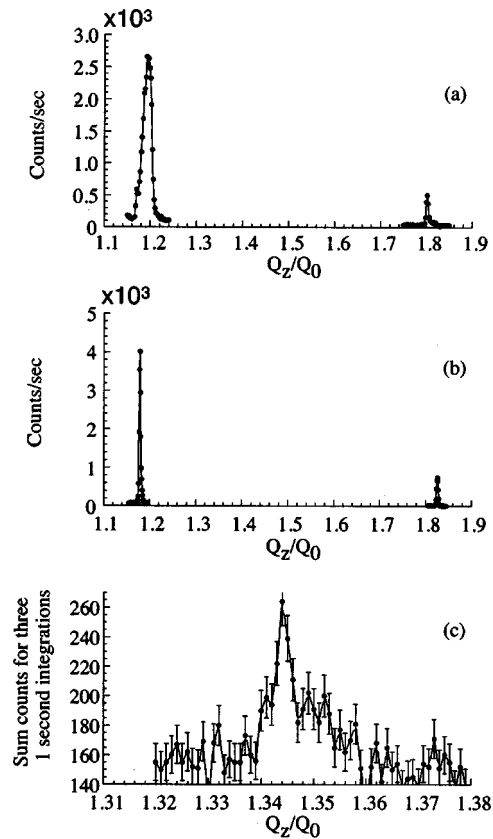


FIG. 11. Resonant peaks in the SmC^*_α phase in (a) compound IV, first order peaks, (b) compound VI, first order peaks, and (c) compound VI, second order peaks.

First, conventional x-ray diffraction experiments on free-standing films of compound VII were performed at low intensity in order to determine the temperature dependence of the layer spacing. Figure 12 gives the evolution of the layer spacing on heating from 79 to 89.5 °C. The layer spacing increases smoothly from 35.55 Å at 79 °C to 36.9 Å at 88 °C and remains constant between 88 and 89.5 °C. The evolution

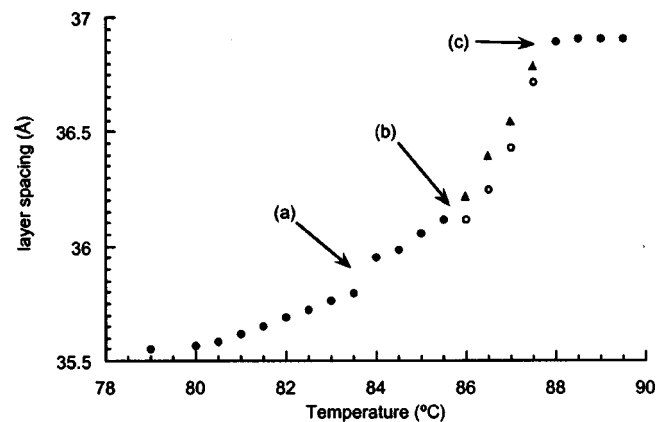


FIG. 12. Evolution of the layer spacing on heating from the SmC^* phase to the SmA phase calculated from the first order peak. The two layer-spacing values (triangle and diamond) in between 88 and 87.5 °C correspond to a split of the first order Bragg peak.

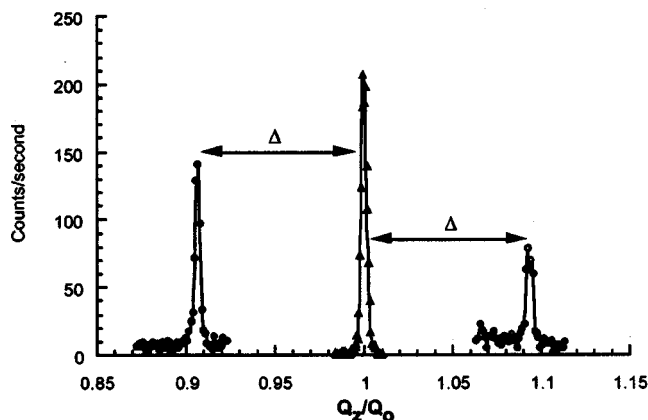


FIG. 13. The resonant satellite on each side of the conventional first order Bragg peak in the SmC_α^* phase at 87.2°C . The first order Bragg peak is observed with attenuators: the attenuation factor in relation to the resonant peak is about 227. Each resonant satellite peak is spaced apart from the first order peak by Δ .

of the layer thickness exhibits three discontinuities, in between (a) 83.5 and 84°C , (b) 85.5 and 86°C , and then (c) 87.5 and 88°C , respectively, as marked in Fig. 12. From this plot, only the high temperature slope discontinuity (c), can be unambiguously attributed to the SmC_α^* - SmA phase transition. According to both resonant scattering data and texture observation of the film, the low temperature jump (a), corresponds to the $\text{SmC}_{\text{FI2}}^*$ - SmC^* phase transition. The third discontinuity (b), is twofold: the slope changes and the first order peak is split above 85.5°C . It is tempting to associate this feature with the SmC^* to SmC_α^* phase transition. Note that the two data points at 86°C indicate the coexistence of two different layer spacings in the irradiated area (Fig. 12). The origin of this splitting remains unclear and may be a surface effect [24] or simply due to different domains in the film sampled by a large beam footprint. Indeed, in this temperature range, the layer spacing and the pitch are rapidly changing with temperature, consequently, a small temperature gradient across the film could produce domains with weak layer-spacing differences. These split layer-spacing peaks are not equal in intensity and their intensity ratios show no particular trend, nevertheless, it should be noted that the split peak region matches the SmC_α^* range.

The resonant scattering study of compound VII was performed in all the SmC^* variant phases but this section focuses on the SmC_α^* and SmC^* temperature ranges. The superlattice periodicity in these phases is deduced from the position of the pair of satellite resonant peaks with respect to the first order Bragg peak (see Fig. 13). Each resonant satellite peak is spaced apart from the first order peak by Δ and the periodicity (helical pitch) is given by $P=1/\Delta$ [where pitch (P) is measured in layer units]. From these data the pitch of compound VII is calculated to be about ten layers at 87.2°C . The first order resonant satellite peaks are observed from 87.4 to 84.1°C and the calculated periodicity varies from about ten layers at high temperature to 75 layers at 84.1°C . Below 84°C the resonant peaks jump to the quarter order positions characteristic of the $\text{SmC}_{\text{FI2}}^*$ phase, hence,

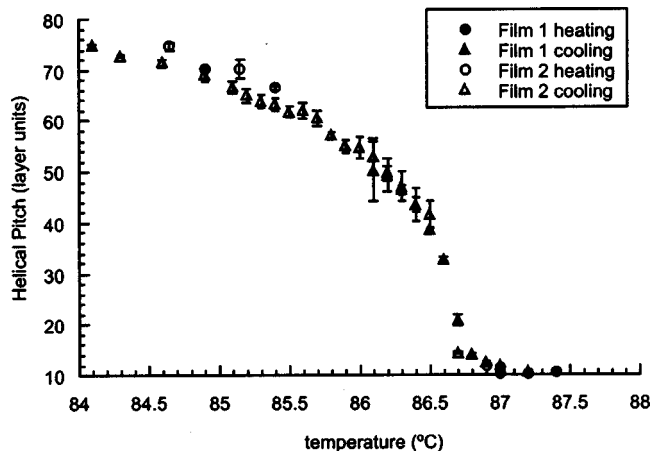


FIG. 14. Evolution of the helical pitch in the SmC_α^* and SmC^* temperature range calculated from the first order resonant satellite peaks. These data are calculated from the splitting of the resonant satellite peaks on two different films of compound VII.

confirming that the low temperature jump (see Fig. 12) corresponds to the $\text{SmC}_{\text{FI2}}^*$ to SmC^* phase transition. The evolution of the helical periodicity throughout the entire SmC_α^* to SmC^* temperature range is plotted in Fig. 14. Two sets of data obtained on two different films are presented in this figure. Note that in the split peak region of the first order peak, the resonant satellite peaks are also sometimes split. In such cases, the average positions of both the split first order peak and the split resonant peak were used to calculate the periodicity. The extreme positions are used to calculate the error bars. The period remains quite constant above 87°C at high temperature, strongly increasing around 86.7°C , the periodicity then smoothly increases to reach 75 layers at 84.1°C in the SmC^* phase. It is difficult to infer from these data whether the evolution of the periodicity exhibits a discontinuity or a vertical slope around 86.7°C . It is interesting to note that from optical observations and the layer-spacing evolution, the temperature of the SmC_α^* to SmC^* transition should be around 86°C ; no discontinuity is visible at this temperature in Fig. 14. At this temperature the periodicity is about 54 layers.

These different resonant scattering results show that the period in the SmC_α^* phase varies from one material to the other. A periodicity of ten layers and more has been observed in this material, compared with five to eight layers in compound VI and five to eight layers in compound IV. These results, however, demonstrate the possibility of a continuous evolution of this period across the SmC_α^* to SmC^* phase transition. An apparent continuity raises questions on the nature of the phase transition and, therefore, of the symmetry of the SmC_α^* phase. Two possibilities must be considered.

(i) The SmC_α^* and SmC^* phases exhibit the same symmetry, i.e., a regular helix. SmC_α^* would correspond to a short pitch (a few layers) whereas SmC^* would have a longer pitch (a few tens to hundreds of layers). The change from SmC^* to SmC_α^* can occur either through a first order transition with a jump in the pitch (which is not detected in our experiments) or with no transition at all through a con-

TABLE I. The expected and confirmed resonant scattering features for the clock model of the SmC^* subphases. “ \times ” indicates features observed in this paper and $\blacksquare\blacksquare$ indicates a feature published previously by the authors [9,10,13,15].

Phase	Superlattice ν	Peak index (L,M)	Expected pol. state (σ incident)	Peak confirmed	Pol. confirmed
SmC_A^*	2	(1,1)	π	$\blacksquare\blacksquare$	$\blacksquare\blacksquare$
		(2,-1)	π	$\blacksquare\blacksquare$	$\blacksquare\blacksquare$
		(1,2)	σ	$\blacksquare\blacksquare$	\times
		(3,-2)	σ	$\blacksquare\blacksquare$	\times
$\text{SmC}_{\text{FI1}}^*$	3	(1,1)	π	$\blacksquare\blacksquare$	
		(2,-1)	π	$\blacksquare\blacksquare$	$\blacksquare\blacksquare$
		(1,2)	σ		
		(2,-2)	σ		
$\text{SmC}_{\text{FI2}}^*$	4	(1,1)	π	$\blacksquare\blacksquare$	$\blacksquare\blacksquare$
		(2,-1)	π	$\blacksquare\blacksquare$	$\blacksquare\blacksquare$
		(1,2)	σ	$\blacksquare\blacksquare$	$\blacksquare\blacksquare$
		(2,-2)	σ	$\blacksquare\blacksquare$	$\blacksquare\blacksquare$
SmC^*	None	(2,-2)	σ	$\blacksquare\blacksquare$	$\blacksquare\blacksquare$
		(2,-1)	π	$\blacksquare\blacksquare$	$\blacksquare\blacksquare$
		(2,1)	π	$\blacksquare\blacksquare$	$\blacksquare\blacksquare$
		(2,2)	σ	$\blacksquare\blacksquare$	$\blacksquare\blacksquare$
		(1,1)	π	$\blacksquare\blacksquare$	$\blacksquare\blacksquare$
SmC_α^*	Incommensurate	(1,1)	π	$\blacksquare\blacksquare$	$\blacksquare\blacksquare$
		(2,-1)	π	$\blacksquare\blacksquare$	
		(1,2)	σ	\times	
		(2,-2)	σ	\times	
SmC_A	2	(1,1)	π	$\blacksquare\blacksquare$	$\blacksquare\blacksquare$
		(2,-1)	π	$\blacksquare\blacksquare$	

tinuous evolution of the pitch. Although consistent with Fig. 14, we rule out this last possibility as a distinct difference between the two phases can be observed in the textures of free-standing films at the transition point.

(ii) If the symmetries of the SmC_α^* and SmC^* phases are different, a second order transition is now permitted. In this case, a symmetry, different from a regular helix must be proposed for the SmC_α^* phase. Simulations of resonant peaks associated with a distorted helix are currently under investigation. The temperature dependence of the periodicity shown in Fig. 14 may be consistent with a second order transition around 86.7 °C.

Our results do not allow an unambiguous distinction between cases (i) and (ii). Case (i) would imply the existence of a period jump too small to be detected. Case (ii) would imply the existence of a new structure, not yet characterized. More careful resonant diffraction experiments are clearly required to look for a period jump [case (i)] or extra resonant satellite peaks [case (ii)].

Note that our results are consistent with optical measurements performed in various materials [19,25] in which different pitch dependencies were reported. Indeed, these measurements have shown that the evolution of the pitch can either be discontinuous at the SmC^* to SmC_α^* phase transition, when the SmC_α^* phase temperature range is large [19] or continuous when the SmC_α^* temperature range is short. In this last case, the SmC_α^* to SmC^* phase transition is quasi-

second order and the pitch typically decreases from 1500 Å to values lower than 500 Å [25]. Note also that for similar values of the pitch, the texture and the thermal behavior of the Friedel fringes differ from the SmC_α^* to the SmC^* phases [18,19,24] perhaps giving evidence of a different symmetry.

In conclusion, these results on compound VII provide information on the evolution of the superlattice periodicity in the SmC_α^* – SmC^* temperature range. Nevertheless, the exact structure of the SmC_α^* phase remains an open question. Further resonant diffraction experiments on this phase should solve this problem.

IV. SUMMARY

A comprehensive study of superlattice layer periodicities in the SmC^* subphases of several liquid crystal materials has been carried out using a resonant x-ray scattering technique at both the selenium and sulphur K -edge energies. In particular, this has allowed the identification of the three- and four-layer structures in the intermediate phases and an interesting investigation of periodicity in the α phase. It has been observed that where two intermediate phases exist in a material’s phase sequence, the three-layer phase always exists at a lower temperature than the four-layer phase. Both the first and second order peaks have been observed in the antiferroelectric, intermediate, ferroelectric, and α phases, reinforcing

theoretical predictions. Further, a direct measurement of the helical pitch in the FI2 phase has been made that agrees well with the only other measurements of pitch in this phase of which we are aware. Table I summarizes fully the features of the clock model that have been revealed previously by x-ray resonant scattering and those that are presented in this paper. The technique has also been broadened to include studies of materials that do not contain a suitable resonant atom in the molecular core.

In the SmC_α^* phase, the layer periodicity of the helical pitch has been measured in some detail across the phase range by an observation of the first order resonant peak locations. This work has revealed a large helical pitch of up to 54 layers in the SmC_α^* phase in compound VII, in contrast to the short pitch of 5.1 layers observed in compound IV and five to eight layers in compound VI [9]. The evolution of this

superlattice periodicity has been considered at the SmC_α^* to SmC^* transition point and raises questions about the nature of this transition and of the symmetry of the SmC_α^* phase.

ACKNOWLEDGMENTS

Work at the Advance Photon Source was supported by the U.S. Department of Energy, Basic Energy Sciences, Office of Energy Research, under Contract No. W-31-109-ENG-38. L.S.H., H.F.G., and S.J.W. thank the Engineering and Physical Sciences Research Council for financial support. L.S.H. also thanks Lucent Technologies for additional financial support. A.C., P.M.J., and C.C.H are grateful for support from the National Science Foundation, Solid State Chemistry Program under Grants Nos. DMR-9703898, 9901739, and INT-9815858.

-
- [1] R. B. Meyer, L. Leibert, L. Strzelecki, and P. Keller, *J. Phys. (Paris)* **36**, L-69 (1975).
 - [2] A. D. L. Chandani, E. Gorecka, Y. Ouchi, H. Takezoe, and A. Fukuda, *Jpn. J. Appl. Phys., Part 1* **28**, 1265 (1989).
 - [3] A. Fukuda, Y. Takanishi, T. Isozaki, K. Ishikawa, and H. Takezoe, *J. Mater. Chem.* **4**, 997 (1994).
 - [4] K. Hiraoka *et al.*, *Jpn. J. Appl. Phys., Part 2* **30**, L1819 (1991); T. Isozaki *et al.*, *Jpn. J. Appl. Phys., Part 1* **31**, 1435 (1992).
 - [5] M. Cepic and B. Zeks, *Mol. Cryst. Liq. Cryst.* **263**, 61 (1995); V. L. Lorman, *ibid.* **262**, 437 (1995); S. A. Piken, S. Hiller, and W. Haase, *ibid.* **262**, 425 (1995); A. Roy and N. Madhusudana, *Europhys. Lett.* **36**, 221 (1996).
 - [6] D. H. Templeton and L. K. Templeton, *Acta Crystallogr., Sect. A: Found. Crystallogr.* **42**, 478 (1986).
 - [7] V. E. Dimitrienko, *Acta Crystallogr., Sect. A: Found. Crystallogr.* **39**, 29 (1983).
 - [8] A. M. Levelut and B. Pansu, *Phys. Rev. E* **60**, 6803 (1999).
 - [9] P. Mach, R. Pindak, A. M. Levelut, P. Barois, H. T. Nguyen, H. Baltes, M. Hird, K. Toyne, A. Seed, J. W. Goodby, C. C. Huang, and L. Furenlid, *Phys. Rev. E* **60**, 6793 (1999).
 - [10] P. Mach, R. Pindak, A. M. Levelut, P. Barois, H. T. Nguyen, C. C. Huang, and L. Furenlid, *Phys. Rev. Lett.* **81**, 1015 (1998).
 - [11] M. Cepic and B. Zeks, *Mol. Cryst. Liq. Cryst.* **263**, 61 (1995).
 - [12] P. M. Johnson, D. A. Olson, S. Pankratz, T. Nguyen, J. Goodby, M. Hird, and C. C. Huang, *Phys. Rev. Lett.* **84**, 4870 (2000).
 - [13] A. Cady, J. A. Pitney, R. Pindak, L. S. Matkin, S. J. Watson, H. F. Gleeson, P. Cluzeau, P. Barois, A.-M. Levelut, W. Caliebe, J. W. Goodby, M. Hird, and C. C. Huang, *Phys. Rev. E* **64**, 050702(R) (2001).
 - [14] V. L. Lorman, *Liq. Cryst.* **20**, 267 (1996).
 - [15] L. S. Matkin, S. J. Watson, H. F. Gleeson, R. Pindak, J. Pitney, P. M. Johnson, C. C. Huang, P. Barois, A.-M. Levelut, G. Srajer, J. Pollmann, J. W. Goodby, and M. Hird, *Phys. Rev. E* **64**, 021705 (2001).
 - [16] Y. Takanishi, K. Hiraoka, V. K. Agrawal, H. Takezoe, A. Fukuda, and M. Matsushita, *Jpn. J. Appl. Phys., Part 1* **30**, 2023 (1991); P. Cluzeau, P. Barois, H. T. Nguyen, and C. Destrade, *Eur. Phys. J. B* **3**, 73 (1998).
 - [17] Y. Takanishi, K. Hiraoka, V. K. Agrawal, H. Takezoe, and A. Fukuda, *Jpn. J. Appl. Phys., Part 1* **30**, 2023 (1991); T. Isozaki, K. Hiraoka, Y. Takanishi, H. Takezoe, A. Fukuda, Y. Suzuki, and I. Kawamura, *Liq. Cryst.* **12**, 59 (1992).
 - [18] V. Laux, N. Isaert, H. T. Nguyen, P. Cluzeau, and C. Destrade, *Ferroelectrics* **179**, 25 (1996).
 - [19] V. Laux, N. Isaert, V. Faye, and H. T. Nguyen, *Liq. Cryst.* **27**, 1, 81 (2000).
 - [20] D. A. Olson, S. Pankratz, P. M. Johnson, A. Cady, H. T. Nguyen, and C. C. Huang, *Phys. Rev. E* **63**, 061711 (2001).
 - [21] W. K. Robinson, H. F. Gleeson, M. Hird, A. J. Seed, and P. Styring, *Ferroelectrics* **178**, 249 (1996).
 - [22] L. S. Matkin, H. F. Gleeson, P. Mach, C. C. Huang, R. Pindak, G. Srajer, J. Pollman, J. W. Goodby, M. Hird, and A. Seed, *Appl. Phys. Lett.* **76**, 1863 (2000).
 - [23] T. Akizuki, K. Miyachi, Y. Takanishi, K. Ishikawa, H. Takezoe, and A. Fukuda, *Jpn. J. Appl. Phys., Part 1* **138**, 4832 (1999).
 - [24] A. Fera, R. Opitz, W. H. de Jeu, B. I. Ostrovskii, D. Schlauf, and Ch. Bahr, *Phys. Rev. E* **64**, 2 (2001).
 - [25] C. Da Cruz, J. C. Rouillon, J. P. Marcerou, and N. Isaert, *Liq. Cryst.* **28**, 125 (2001).